Adsorption of Molecular Brushes with Polyelectrolyte Backbones onto Oppositely Charged Surfaces: A Self-Consistent Field Theory

ARTICLE *in* LANGMUIR · AUGUST 2008

Impact Factor: 4.46 · DOI: 10.1021/la800272v · Source: PubMed

4 AUTHORS, INCLUDING:

Frans A M Leermakers
Wageningen University
288 PUBLICATIONS **4,741** CITATIONS
SEE PROFILE

Marcus Textor
ETH Zurich
333 PUBLICATIONS **13,999** CITATIONS
SEE PROFILE

Adsorption of Molecular Brushes with Polyelectrolyte Backbones onto Oppositely Charged Surfaces: A Self-Consistent Field Theory

Laurent Feuz,[†] Frans A. M. Leermakers,[‡] Marcus Textor,[†] and Oleg Borisov*[,§]

Laboratory for Surface Science and Technology, Department of Materials, ETH Zurich, Wolfgang-Pauli-Strasse 10, CH-8093 Zurich, Switzerland, Laboratory of Physical Chemistry and Colloid Science, Wageningen University, Dreijenplein, 6, 67003 HB Wageningen, The Netherlands, and Institut Pluridisciplinaire de Recherche sur l'Environnement et les Matrériaux, UMR 5254, UPPA CNRS, 64053 Pau, France

Received January 26, 2008. Revised Manuscript Received March 21, 2008

The two-gradient version of the Scheutjens−Fleer self-consistent field (SF-SCF) theory is employed to model the interaction between a molecular bottle brush with a polyelectrolyte backbone and neutral hydrophilic side chains and an oppositely charged surface. Our system mimics *graft*-copolymers with a cationic main chain (among which poly(L-lysine)-*graft*-poly(ethylene glycol) (PLL-*g*-PEG) or poly(L-lysine)-*graft*-polyoxazoline are well-known examples) interacting with negatively charged (metal oxide) solid surfaces. We aim to analyze the copolymer−surface interaction patterns as a function of the molecular architecture parameters. Two regimes are investigated: First, we compute the effective interaction potential versus the distance from the surface for individual bottle brush macromolecules. Here, depending on the grafting ratio and the degree of polymerization of the side chains, the interplay of electrostatic attractions of the main chain to the surface and the steric repulsion of the grafts results in different patterns in the interaction potential and, therefore, in qualitatively different adsorption behavior. In particular, we demonstrate that, at high side chain grafting density and short grafts, the molecular brushes are strongly adsorbed electrostatically onto negatively charged substrates, whereas, in the opposite case of low grafting ratio and high molecular weight of grafts, the steric repulsion of the side chains from the surface dominates the polymer−surface interaction. At intermediate grafting ratios, the adsorption/depletion scenario depends essentially on the ratio between the electrostatic screening length and the thickness of the molecular bottle brush. We further have analyzed the equilibrium adsorbed amount as a function of the macromolecular architecture. Our results are based on a detailed account of attractive and repulsive (including *inter*molecular in-plane) interactions, and suggest a nonmonotonic dependence of the adsorbed amount on the grafting ratio, in good agreement with the experimental studies for PLL-*g*-PEG adsorption onto Nb_2O_5 surfaces. The results of the theoretical modeling are discussed in the context of the optimization of the PLL-*g*-PEG molecular design parameters in order to create protein-resistant surfaces.

I. Introduction

The self-assembly of poly(ethylene glycol) (PEG)-based copolymers at the water−solid interface is a widely used tool for surface modifications aimed to improve their biointeractive (e.g., protein-resistant) or lubrication properties in aqueous media.[1] The development of protein-resistant surfaces (prevention of nonspecific protein adsorption) is of central interest in the context of the design of biosensor chips and medical implants that must operate in contact with blood.

A particular class of macromolecules is based on a poly(L-lysine) (PLL) main chain, charged positively at a neutral pH because of the presence of protonated amine groups, and decorated by grafted PEG side chains (PLL-*g*-PEG).[2] The polyelectrolyte nature of the PLL main chain (backbone) evokes Coulomb attraction as the driving force of the adsorption of PLL-*g*-PEG monolayers at negatively charged metal oxide surfaces. Recently, other but conceptually similar types of *graft*-copolymers with a cationic main chain and water-soluble grafts, e.g., poly(ethylene oxide)[3] or polyoxazoline,[4] have been explored with respect to their adsorption behavior and protein resistance. In spite of this rapidly growing experimental activity, to the best of our knowledge there are no theoretical studies on electrostatically driven adsorption of bottle brushes with polyelectrolyte main chains.

The ultimate goal of experimental and theoretical research in this domain of biomaterial science is to establish a systematic relation between the macromolecular architecture of the copolymers (molecular weights, grafting ratio), the structure of the adsorbed copolymer monolayer, and its resistance to nonspecific protein adsorption. To rationalize structure−property relations, insight in the hierarchy of *intra*- and *inter*molecular interactions in the protective polymer monolayer is required, including the interactions with the substrate and with protein molecules.

The generic model assumes that the protein repellent properties of PEG-modified interfaces are the result of a shielding of the bare surface by an "inert", highly hydrated PEG layer. Nowadays, this model is widely accepted and well-supported by numerous experimental studies on surfaces modified by PEG or by other water-soluble nonionic polymers, e.g. polyoxazolines, and essentially explains protein resistance following the same physical principles as the classical theory of steric stabilization of colloidal dispersions by polymers. The main qualitative trends predicted on the basis of a simple scaling-type approach[5] are in line with

* To whom correspondence should be addressed. E-mail: oleg.borisov@univ-pau.fr. Tel: +33-559-40-75-91. Fax: +33-559 40 76 23.
[†] ETH Zurich.
[‡] Wageningen University.
[§] UPPA CNRS.

(1) Harris, J. M. *Poly(ethylene glycol) Chemistry: Biotechnical and Biomedical Applications*; Plenum Press: New York/London, 1992.
(2) Pasche, S.; De Paul, S. M.; Vörös, J.; Spencer, N. D.; Textor, M. *Langmuir* **2003**, *19*(22), 9216–9225.
(3) Pettersson, T.; Naderi, A.; Makuska, R.; Claesson, P. M. *Langmuir* **2008**, *24*(7), 3336–3347.
(4) Konradi, R.; Pidhatika, B.; Muhlebach, A.; Textort, M. *Langmuir* **2008**, *24*, 613–616.
(5) Halperin, A. *Langmuir* **1999**, *15*(7), 2525–2533.

10.1021/la800272v CCC: $40.75
Published on Web 06/18/2008

results of detailed calculations of protein−brush interactions performed on the basis of the single-chain self-consistent field (SCF) method by Szleifer.[6,7] A more advanced theoretical model proposed recently by Halperin[8,9] allows for weak attractive interactions between PEG chains forming the brush and protein globules, giving rise to ternary adsorption of proteins in the brush. In this case, the protein adsorption patterns may be rationalized in terms of the model of "polymer brush with annealed excluded volume interactions".[10,11] Unfortunately, to date, the available experimental data do not allow one to quantify the PEG−protein interaction parameters unambiguously.

Very effective protective polymeric layers can be made by anchoring or end-grafting water-soluble PEG chains at the interface, i.e., by creating a PEG brush. In such a brush, individual chains are strongly overlapping. This means that the distance between chains is small with respect to the coil size and, even more relevant for the application as nonfouling surfaces, with respect to the size of the protein globule. The latter ensures a strong steric repulsion (of entropic origin) upon the penetration of a protein globule into the layer. An essential feature of brushes in a good solvent (that is, the case for PEG in water at ambient conditions) is the swelling (hydration) of the brush by the good solvent (water), and the strong stretching of its chains, which is responsible for the strong repulsion felt by the protein globule upon its penetration into the brush.

In spite of significant progress in *grafting to* and particularly *grafting from* methods to obtain regular and dense polymeric brushes, the applicability of these methods for PEG brushes is very limited (there is no known route for *grafting from*; known methods are nontechnological for *grafting to*). More sophisticated approaches, e.g., cross-linking of end-functionalized star-shaped PEG immobilized at the surface, enable one to obtain specifically biofunctionalized surfaces, which exhibit excellent resistance with respect to nonspecific protein adsorption.[12]

The self-assembly approach using PEG-based copolymers remains most relevant due to its simplicity and technological viability. Typically, *diblock*-copolymers, comprising PEG blocks linked to "anchor" blocks, represent a generic type of copolymers that, by assembling, give rise to PEG brushes that are relatively unstable and can detach from the surface upon variation of the environmental conditions (including washing with pure solvent) or by some mechanical stress.[13–15]

The *graft*-copolymers, however, with a sufficiently long anchoring main chain bearing multiple PEG grafts, offer an attractive alternative because of their much larger net adsorption energy, making adsorption in experimentally relevant situations virtually irreversible.

In contrast to *diblock*-copolymer adsorption, the interaction of a *graft*-copolymer with the surface is governed by a delicate balance of *intra*- and *inter*molecular attractive and repulsive forces (electrostatic, Van der Waals), each with its particular range and strength, modulated by the presence of an adsorbing surface. Altogether, as we will demonstrate below, this interplay results in a quite complex pattern in the net profiles for the interaction potential of the polymer with the surface and in the structure of the adsorbed monolayer.

Our main goal is to rationalize the adsorption behavior of the molecular brushes with polyelectrolyte backbone and neutral water-soluble grafts in terms of the relation between the copolymer architecture, the shape of the profile for the effective interaction of the polymer with the surface (interaction curve), and the structure of the adsorbed polymer monolayers. In addition, we will compare our predictions with available experimental results.

While the theory of electrostatically driven adsorption of polyelectrolytes onto oppositely charged surfaces[16–23] and the theory of the conformation of nonionic molecular bottle brushes in solutions[24–27] are relatively well established, no models are available to describe the conformations of nonionic molecular bottle brushes with a charged main chain near an oppositely charged surface. Even though we employ various simplifications, the system remains too complex for the description by analytical theory. Therefore, we here use a numerical SCF approach.

The remainder of the paper is organized as follows: in Section II we present and justify our simplified model for the analysis of interactions between a molecular bottle brush with a polyelectrolyte backbone and neutral grafts with an oppositely charged solid surface by means of a two-gradient Scheutjens−Fleer SCF (SF-SCF) approach. The implementation issues of the computational approach are described in Section III (the basics of the model are given in the Appendix). In Section IV, the effective potential profiles for individual macromolecules and an oppositely charged surface are analyzed. The multichain problem, i.e., the structure of the adsorbed layer, is considered in Section V. We summarize our findings and compare these to the experimental results for PLL-*g*-PEG adsorption onto Nb_2O_5 in Section VI.

II. Molecular Brush with Polyelectrolyte Main Chain in Solution

We start with a brief discussion of the conformation of molecular brushes with a polyelectrolyte main chain and water-soluble nonionic grafts, mimicking PLL-*g*-PEG-type copolymers in aqueous solution. The molecular brushes that are under consideration here consist of a main polyelectrolyte chain to which at intervals nonionic side chains are attached. In Figure 1 we present the typical architecture of PLL-*g*-PEG copolymers exemplifying the ionic/nonionic molecular brushes. The average number of the main chain monomers per one graft, $g \geq 1$, is called the grafting ratio and characterizes the density of grafting in the molecular brush. Together with the number of monomer

(6) Linse, P.; Bjorling, M. *Macromolecules* **1991**, *24*(25), 6700–6711.
(7) Szleifer, I. *Biophys. J.* **1997**, *72*(2), 595–612.
(8) Halperin, A.; Fragneto, G.; Schollier, A.; Sferrazza, M. *Langmuir* **2007**, *23*, 10603–10617.
(9) Jeon, S. I.; Lee, J. H.; Andrade, J. D.; De Gennes, P. G. *J. Colloid Interface Sci.* **1991**, *142*(1), 149–158.
(10) Currie, E. P. K.; Fleer, G. J.; Stuart, M. A. C.; Borisov, O. V. *Eur. Phys. J. E* **2000**, *1*(1), 27–40.
(11) Currie, E. P. K.; Van der Gucht, J.; Borisov, O. V.; Stuart, M. A. C. *Pure Appl. Chem.* **1999**, *71*(7), 1227–1241.
(12) Heyes, C. D.; Groll, J.; Moller, M.; Nienhaus, G. U. *Mol. Biosyst.* **2007**, *3*(6), 419–430.
(13) Bearinger, J. P.; Terrettaz, S.; Michel, R.; Tirelli, N.; Vogel, H.; Textor, M.; Hubbell, J. A. *Nat. Mater.* **2003**, *2*(4), 259–264.
(14) Feller, L. M.; Cerritelli, S.; Textor, M.; Hubbell, J. A.; Tosatti, S. G. P. *Macromolecules* **2005**, *38*(25), 10503–10510.
(15) Lee, J. H.; Kopecek, J.; Andrade, J. D. *J. Biomed. Mater. Res.* **1989**, *23*(3), 351–368.
(16) Wiegel, F. W. *J. Phys. A: Math. Gen.* **1977**, *10*(2), 299–303.
(17) Dobrynin, A. V.; Deshkovski, A.; Rubinstein, M. *Phys. Rev. Lett.* **2000**, *84*(14), 3101–3104.
(18) Podgornik, R. *J. Phys. Chem.* **1992**, *96*(2), 884–896.
(19) Varoqui, R. *J. Phys. II* **1993**, *3*(7), 1097–1108.
(20) Chatellier, X.; Joanny, J. F. *J. Phys. II* **1996**, *6*(12), 1669–1686.
(21) Joanny, J. F. *Eur. Phys. J. B* **1999**, *9*(1), 117–122.
(22) Borisov, O. V.; Zhulina, E. B.; Birshtein, T. M. *J. Phys. II* **1994**, *4*(6), 913–929.
(23) Borisov, O. V.; Boulakh, A. B.; Zhulina, E. B. *Eur. Phys. J. E* **2003**, *12*(4), 543–551.
(24) Birshtein, T. M.; Borisov, O. V.; Zhulina, Y. B.; Khokhlov, A. R.; Yurasova, T. A. *Polym. Sci. U.S.S.R.* **1987**, *29*(6), 1293–1300.
(25) Zhulina, Y. B. *Polym. Sci. U.S.S.R.* **1984**, *26*(4), 885–891.
(26) Zhulina, Y. B.; Birshtein, T. M. *Polym. Sci. U.S.S.R.* **1985**, *27*(3), 570–578.
(27) Bug, A. L. R.; Cates, M. E.; Safran, S. A.; Witten, T. A. *J. Chem. Phys.* **1987**, *87*(3), 1824–1833.

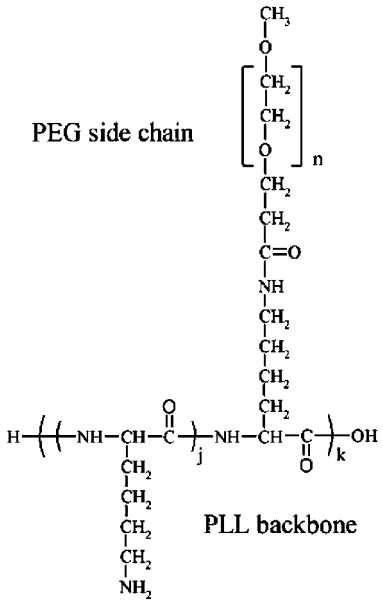

Figure 1. Chemical structure of the PLL-*g*-PEG copolymer, where, by variation of the parameters *j* (related to the grafting ratio), *k* (related to the PLL molecular weight), and *n* (related to the PEG molecular weight), different polymer architectures can be obtained.

units, *n*, per graft and the total number of monomer units in the main chain, $(j + 1)k$, the grafting ratio *g* completely characterizes the macromolecular architecture. Here and below we assume $g < n$. This ensures the strong crowding of the neighboring grafts, and it allows us to classify and to treat the graft copolymers as molecular brushes.

Both PEG and PLL chains are intrinsically flexible, that is, the statistical segment length (for PLL, the latter is defined in the nonprotonated, neutral state) is close to the monomer unit size, that is, on the order of $0.5 \div 0.75$ nm. Each monomer unit of the PLL chain that does not carry a PEG graft can ionize via protonation. This occurs at a sufficiently low pH of the solution ($pK \approx 8.5$). Hence, at physiological (neutral pH) conditions, the PLL backbone is a strongly dissociated polyelectrolyte with a fixed fraction $\alpha = (g - 1)/g$ of charged monomer units.

Conformations of the molecular brushes with polyelectrolyte backbones are strongly affected by the superposition of the electrostatic repulsion between ionized monomer units of the main chain (the polyelectrolyte effect) and the steric repulsion between the crowded grafts (the molecular brush effect). The former depends on the fraction α of ionic monomers in the main chain that can be tuned by varying the ionic strength and pH in the solution, whereas the latter is determined by the grafting density and the solvent strength conditions for the side chains. Water under ambient conditions is a good solvent for ethylene glycol (EG) monomers, but its quality as a solvent decreases upon an increase in temperature (so-called lower critical solution temperature (LCST) behavior is typical for nonionic water soluble polymers).[28] The superposition of both Coulombic and steric repulsions induces an axial tension in the backbone of the molecular brush. As has been extensively discussed in the literature,[24,29–31] this tension results in the stretching of the main chain on a length scale controlled by the corresponding interaction ranges. Since a decrease in steric repulsion upon an increase in the grafting ratio is compensated by an increase in the Coulomb repulsion due to a simultaneously increasing fraction of charged monomer units in the main chain, for PLL-*g*-PEG type copolymers this axial tension and, as a result, the stretching of the backbone persist in a wide range of grafting ratios.[32]

The characteristic range of electrostatic interactions is given by the Debye screening length, whereas for steric interactions it is controlled by the characteristic extension of the grafts. Furthermore, sufficiently strong repulsions may give rise to an induced bending rigidity of the molecular brushes that manifests on length scales exceeding the characteristic interaction ranges.[30,33–35] Remarkably, due to thermal fluctuations, the main chain remains randomly bent on a local length scale, whereas the induced rigidity manifests in large-scale conformational properties (e.g., gyration radius) of the molecular brushes. As has been demonstrated for nonionic molecular brushes, the effect of the induced bending rigidity of the bottle brush arising as a result of crowding and repulsion of the grafts is reduced by the repartitioning of a fraction of the side chains from the concave to the convex side of the brush upon bending.[24,36,37] For experimentally relevant copolymer architectures, the molecular brush as a whole thus preserves local cylindrical symmetry on the length scale of the order of its characteristic thickness, *D* (the latter is controlled by radial extension of the grafts). This is in agreement with recent SANS studies of the PLL-*g*-PEG molecular brushes in solution.[38] Therefore, one does not expect the manifestation of lyotropic order in a solution even at sufficiently high copolymer concentrations. However, due to additional steric constraints imposed for side chains near a surface, the induced rigidity effects may in fact become more important in a monolayer of molecular brushes adsorbed onto the surface, and this can possibly lead to the appearance of some local orientational order.

III. SF-SCF Numerical Modeling: Implementation Issues for Calculations

The method of Scheutjens and Fleer is a powerful, numerical SCF computational approach that allows for the investigation of both structural and mechanical properties of molecular bottle brushes and their interactions with interfaces. A significant advantage of the SF-SCF calculation is its very high computational efficiency, while obtaining practically the same accuracy as Monte Carlo (MC) and molecular dynamics (MD) methods. In addition, mechanical properties, such as the bending rigidity of the molecular brush, can directly be retrieved from the partition function, whereas in MC simulations, they are only indirectly accessible. Using the SF-SCF method, we can analyze conformations of the bottle brushes with a high grafting density and long side chains and go beyond the limits of MC or MD methods. An important drawback of the available SCF algorithm is, however, its inability to account for all gradients of the local properties in the system. More specifically, the analysis is limited to gradients in two directions, which imposes a certain type of symmetry for the system under consideration. A description of the computational model is given in the Appendix.

(28) Aseyev, V. O.; Tenhu, H.; Winnik, F. M. *Conformation-Dependent Design of Sequences in Copolymers II*; Springer-Verlag: New York, 2006; Vol. *196*, pp 185.
(29) De Gennes, P. G. *J. Phys.* **1976**, *37*(12), 1445–1452.
(30) Khokhlov, A. R.; Khachaturian, K. A. *Polymer* **1982**, *23*(12), 1742–1750.
(31) Borisov, O. V.; Birshtein, T. M.; Zhulina, Y. B. *Polym. Sci. U.S.S.R.* **1987**, *29*(7), 1552–1559.
(32) Feuz, L. Thesis ETH Zürich No. 16644, 2006, http://e-collection.ethbib.ethz.ch/view/eth:28807.
(33) Odijk, T. *J. Polym. Sci., Part B: Polym. Phys.* **1977**, *15*(3), 477–483.
(34) Skolnick, J.; Fixman, M. *Macromolecules* **1977**, *10*(5), 944–948.
(35) Odijk, T. *Macromolecules* **1979**, *12*(4), 688–693.
(36) Fredrickson, G. H. *Macromolecules* **1993**, *26*(11), 2825–2831.
(37) Feuz, L.; Leermakers, F. A. M.; Textor, M.; Borisov, O. *Macromolecules* **2005**, *38*(21), 8891–8901.
(38) Feuz, L.; Strunz, P.; Geue, T.; Textor, M.; Borisov, O. *Eur. Phys. J. E* **2007**, *23*(3), 237–245.

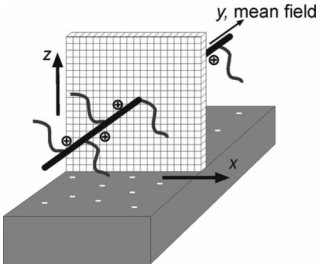

Figure 2. Schematic view of the computational model of a *graft*-copolymer with polyelectrolyte backbone near an oppositely charged planar surface in the two-gradient flat coordinate system. The polyelectrolyte backbone of the macromolecule is kept in a straight configuration along the *y*-axis of the system. The gradients read along the *x* and *z* coordinates, whereas all the local properties (densities) are assumed to be constant along the *y*-axis.

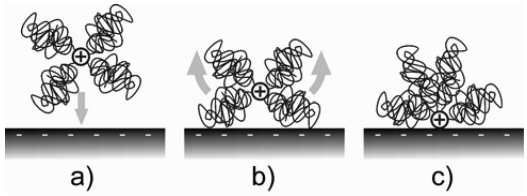

Figure 3. Schematic view of the cross-section perpendicular to the backbone of a *graft*-copolymer molecule approaching a surface, as done in the SF-SCF calculations in this section. (a) Unconfined molecule not interacting sterically with the surface. (b) Onset of steric interactions with the surface, involving the rearrangement of the side chains due to confinement by the surface. (c) *Graft*-Copolymer molecule adsorbed onto a surface: the backbone lies flat on the surface. In SF-SCF calculations, the *z*-value for the backbone of the molecule is imposed, and then the free energy (effective polymer−surface interaction potential) is calculated for the particular configuration.

The primary aim of our analysis is to rationalize the adsorption data for PLL-*g*-PEG molecular brushes. Thus, we assimilated (within the resolution of the coarse-graining scheme) our computational model to this particular type of ionic/nonionic molecular brushes.

Since the SCF modeling scheme applied in our calculations enables one to account for gradients in polymer density and self-consistent potential along two coordinates only, we approximate the molecular brushes as an array of flexible chains, end-grafted onto a uniformly charged line; the latter mimicking the extended polyelectrolyte backbone. As discussed in Section II, a significant extension of the main chain arises because of the superposition of steric and electrostatic repulsions and therefore persists in a wide range of variation of the grafting ratio. As the chains bear multiple grafts on a length comparable to the thickness of the bottle brush, we can safely neglect the flexibility of the main chain in the modeling of the adsorption of the bottle brush to the surface.

Furthermore, because of the same symmetry reasons, we only account for those configurations wherein the backbone is parallel to the surface.

We use a two-gradient flat lattice geometry with the pair of coordinates (x,z), introducing an impermeable surface at one of the system borders (see Figure 2). For this particular lattice geometry, the normalization constant of eq A6 is given by $C = 1/g$. The lattice unit cell size a is set to 0.5 nm. Hence, within our discretization scheme, each monomer unit occupies a lattice site of size 0.5 nm, which is close to the dimensions of either an ethylene oxide or an L-lysine monomer unit. For infinitely long bottle brushes in the straight-backbone configuration, we may ignore the end-cap effects.

We stress that we perform the calculations for the grafted side chains, while we apply a mean-field approximation along the main chain direction. The input parameters thus always refer to the side chains, and the fact that they are grafted to a main chain is only reflected through the side chain density per unit length in the direction of the main chain (or mean field). The program used for this analysis has been developed at the Wageningen University, Netherlands, and is called SFbox.[39]

Although the two-gradient SF-SCF calculations are efficient in CPU time, the memory usage may become limiting, e.g., for very large arms (such systems need a large simulation space). To optimize the range of molecular weights that can be considered, in the case of a bottle brush in solution one may make use of the symmetry of the problem. As the reflecting (Neuman) boundary conditions on all system boundaries are implemented, one can pin the arms of the bottle brush to the coordinate $\mathbf{r}^* = (1,z^*)$ and consider only one-half of the bottle brush to be in the system; the mirror image corresponds then to the other side of the system boundary.

In the first part, we are interested in the polymer−surface effective interaction potential, computed by bringing the polymer step-by-step closer to the surface. More specifically, the PLL backbone is pinned at a certain distance z from the surface, and the equilibrium conformation is calculated for this situation. Then, the backbone is moved to a smaller distance z, and calculations are run again. This is repeated until the backbone lies on the surface (Figure 3).

We calculate the change in free energy upon interaction with the surface with respect to the situation where the copolymer is far away from the surface. In the latter case, the copolymer is not confined by the surface, and its free energy is independent of its distance z from the surface, and can be taken as a reference state ($F^{\mathrm{po}}_{\mathrm{ref}}$). Hence, the values shown in the plots are obtained by subtracting the free energy value for the unconfined polymer from the value obtained for a certain distance z from the surface.

$$\Delta F^{\mathrm{po}}(z) = F^{\mathrm{po}}(z) - F^{\mathrm{po}}_{\mathrm{ref}} \tag{1}$$

Note that one of the main constraints imposed in this section is the parallel and straight conformation of the polyelectrolyte backbone with respect to the surface plane, i.e., the neglect of fluctuations of the polyelectrolyte backbone on the length scale $< D$.

In the second part, we will mimic the lateral crowding of the molecules on the surface by taking advantage of the mirror boundary conditions, i.e., there is always another "phantom" molecule on the other side of the boundary (Figure 4a). We believe that, because of the mutual impermeability of molecular brushes (see corresponding discussion in ref 31), the local packing in the adsorbed layer corresponds to a parallel alignment of segments of adsorbed molecular brushes, whereas crossing configurations are costly and therefore relatively rare. Of course, on the large scale, sufficiently long molecular brushes acquire randomly bent in-plane conformations.

By reducing step-by-step the width of the simulation box (Figure 4b), the surface concentration of chains increases. Finally, for small box widths, the side chains will be confined, i.e., we can actually engender the interaction between chains of neighboring molecules (Figure 4c). The expected curve showing the change in free energy per unit area upon crowding is schematically shown in Figure 4d.

(39) van Male, J. Self-Consistent-Field Theory for Chain Molecules: Extensions, Computational Aspects, and Applications. Doctoral Thesis, Wageningen University, 2003.

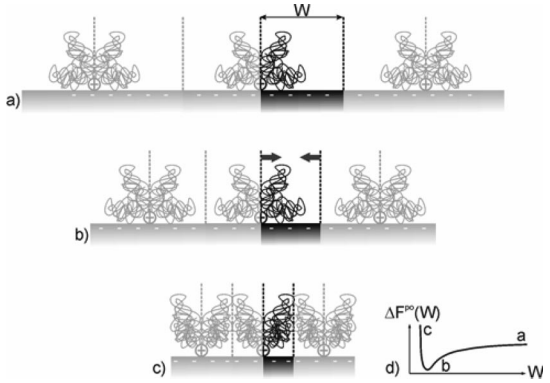

Figure 4. Schematic illustration of the lateral crowding of *graft*-copolymer molecules in the adsorbed monolayer mimicked by the SF-SCF technique. The backbone is lying flat on the surface (perpendicular to the drawing plane). The calculation box area is drawn in black, while the gray parts show the "phantom" molecules that are present as a result of mirror boundary conditions. (a) Situation of the laterally unconfined molecules (dilute surface regime). (b) Decreasing the box width (just before lateral interactions). (c) Crowding and interaction of neighboring side chains (semidilute surface regime). (d) Schematic curve of the free energy per unit area vs the box width. The letters in the plot correspond to situations a, b, and c of the schematic drawings. The minimum in the curve corresponds to the thermodynamically optimal crowding condition.

The lateral size of the system W (which equals half the lateral distance between backbones) was varied from 15 down to 0.5 nm (from 30 down to 1 lattice cell size) and the free energy was calculated for each system width. As a reference state, the free energy of the unconfined molecule far away from the surface (z = 30 nm) was calculated.

From all the free energy values, the (system width dependent) total excess surface free energy, γW, was subtracted, where γ is the bare interfacial free energy per unit area. The resulting free energy was then normalized by the system width W in order to get the free energy per surface area:

$$F^{po}(W) = \frac{(F^{po}_{z=0.5nm}(W) - \gamma W) - (F^{po}_{z=30nm} - \gamma W_{z=30nm})}{W} \quad (2)$$

where F^{po} is the partial open free energy of the adsorbed monolayer per unit area, $F^{po}_{z=0.5nm}$ is the output of the SCF calculations for the adsorbed molecule (backbone contacts the surface), $F^{po}_{z=30nm}$ is the output of the SCF calculations for the unconfined molecule, γ is the surface excess free energy, W is the system width, and $W_{z=30nm}$ is the system width for the unconfined molecule calculation.

The surface excess free energy γ has been determined by calculating the free energy of the system as a function of the width W in the absence of the polymer. It is only a function of the salt concentration and the surface charge (for simplicity, the ions do not have a specific adsorption energy).

The equilibrium adsorbed amount (optimal surface coverage) is determined from the condition of minimum of the excess free energy given by eq 2 as a function of the box size W. We remark that this is an approximation corresponding to the plateau regime in the adsorption isotherms, where the concentration dependence of the adsorbed amount is negligible.

IV. Effective Interaction Potential of a Single Molecular Brush with a Surface

The effective interaction potential U (to be distinguished from the segmental self-consistent potentials u) between a molecular brush with a polyelectrolyte backbone and an oppositely charged surface comprises four main contributions:

- $U_{Coulomb}$: *Coulomb attraction* due to the opposite charges on the surface and on the polyelectrolyte backbone
- U_{VdW}: *nonelectrostatic, short-range Van der Waals attraction* between monomer units and the surface
- U_{conf}: effective *entropic repulsion* due to the reduced number of possible *conformations* for single side chains (important at large grafting ratios)
- U_{steric}: effective *steric repulsion* due to the *confinement* of the bottle brush (enhanced *intra*brush steric interactions; important at small grafting ratios)

There may be an additional (Coulomb) repulsive contribution due to the image charge effect, but it will not be treated here because it is only relevant for surfaces with low dielectric constants, which in not the case in this study. It is also worth mentioning that, except for the nonelectrostatic short-range attraction, all the potentials act (and compete) on a mesoscopic length scale. These contributions then add up to the total potential $U(z)$.

$$U(z) = U_{VdW}(z) + U_{Coulomb}(z) + U_{conf}(z) + U_{steric}(z) \quad (3)$$

Hence, the total potential experienced by a *graft*-copolymer (and presented here per monomer of the main chain, i.e., per segment of 0.5 nm length of the molecular brush) is governed by an interplay of attractive and repulsive forces. Depending on the relative importance of these contributions, either attraction (leading to polymer adsorption) or repulsion (leading to depletion of the polymer from the surface) may dominate.

We start with the analysis of the individual contributions in the polymer−surface interactions, presented in eq 3 and then consider the net interaction potential patterns.

IV.1. Non-Electrostatic, Short-Range Van der Waals Attraction. The nonelectrostatic, short-range Van der Waals attraction can be presented as

$$U_{VdW}(z) \approx \mu\delta(z) \quad (4)$$

where μ is the contact interaction energy, and $\delta(z)$ is the one-side Dirac delta function. As the term "contact" already suggests, this potential acts only in the very proximity of the surface (<1 nm). It can in principle act on both components of the bottle brush, i.e., the backbone and the side chains. It is essentially insensitive to ionic strength, but it may depend on the ionization state of the chain and play a major role in the adsorption of neutral polymers. We remark that there are no quantitative experimental reports on short-range attractive forces between, e.g., PEG and metal oxide surfaces in aqueous solutions. We will neglect this quantity in our calculations, but keep in mind that it can have a certain influence on the adsorption behavior and stability of the copolymer layer on the surface.

IV.2. Coulomb Attraction. The Coulomb attraction potential $U_{Coulomb}(z)$ depends on the linear charge density along the polymer backbone as well as on the ionic strength of the solution and the surface charge density.

The analytical calculation of the Coulomb contribution to the interaction free energy between the polyelectrolyte backbone and the charged surface requires a solution of the Poisson−Boltzmann (PB) equation for a line charge near an oppositely charged (infinite) plane, which is not available.

The results of the SCF calculations for the free energy of a charged line (mimicking the polyelectrolyte backbone) approaching an oppositely charged surface are presented in Figure 5a. The surface charge density (in numbers of elementary charges) was assumed as -1.3 nm^{-2} (based on AFM results by Pasche

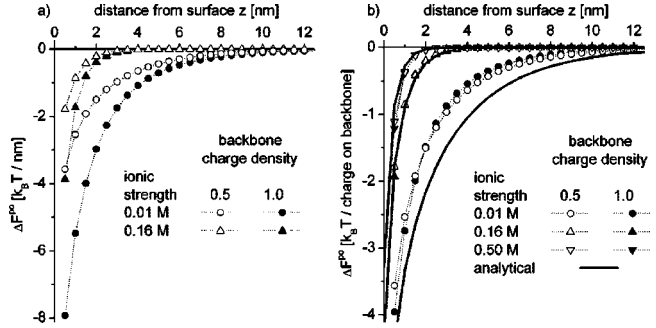

Figure 5. (a) Gain in free energy of a charged line (per nanometer along the line) for different charge densities upon approaching an oppositely charged surface. (b) Same data as in panel a, but normalized per charge on the backbone. Additionally, values calculated for salt concentration equal to 0.50 M and analytical curves (solid lines) are plotted.

et al.[40] for Nb_2O_5). Two charge densities along the backbone were chosen: $\alpha = 1$, representing a fully protonated polycationic main chain, and $\alpha = 0.5$, mimicking the charge density present on a copolymer with high grafting density. The ionic strengths of 0.01 and 0.16 M correspond to usual conditions used in experimental work.

Obviously, a positively charged backbone experiences a net attraction when approaching an oppositely charged surface. Indeed, this can be seen for all the calculated cases in Figure 5. The magnitude of the attractive force increases with (i) higher charge density of the backbone and (ii) lower ionic strength.

When dealing with charged surfaces, one has to introduce the so-called Gouy−Chapman length. It describes the distance from the charged surface, in which the counterions are localized in a salt free solution, i.e., the distance at which the electrical charge of the surface exerts a significant influence. The Gouy−Chapman length λ is defined as $\lambda = 1/(2\pi l_B \sigma)$, where l_B is the Bjerrum length (defined below), and σ is the surface charge density, given in the number of elementary charges per unit area. The Bjerrum length $l_B = e^2/\varepsilon k_B T$ is the characteristic length scale at which the electrostatic interaction between a pair of monovalent ions has the magnitude of the thermal energy $k_B T$. ε is the dielectric constant of the solvent.

The reduced (dimensionless) electrostatic potential $\psi(z) = e\Psi(z)/k_B T$ (e being the elementary charge) at a distance $z \geq 0$ is given by

$$\psi(z) = \pm 2\ln\Big[r_D^{-1}\lambda + \sqrt{r_D^{-2}\lambda^2 + 1} - 1 + \Big(r_D^{-1}\lambda - \sqrt{r_D^{-2}\lambda^2 + 1} + 1\Big)\exp(-r_D^{-1}z)\Big] \Big/ \Big[r_D^{-1}\lambda + \sqrt{r_D^{-2}\lambda^2 + 1} - 1 - \Big(r_D^{-1}\lambda - \sqrt{r_D^{-2}\lambda^2 + 1} + 1\Big)\exp(-r_D^{-1}z)\Big] \quad (5)$$

where $r_D = (4\pi l_B \Sigma c_{ions}^N \nu^2)^{-1/2}$ is the Debye length, c_{ions}^N is the ion number density per volume, and υ is the ion valency. The signs "+" and "−" in eq 5 refer to positively and negatively charged surfaces, respectively. Equation 5 has the following asymptotics: at $r_D^{-1}\lambda < 1$ (low salt limit)

$$\psi(z) \approx \mp 2\ln\left(\frac{r_D^{-1}\lambda}{2} + \tanh\frac{r_D^{-1}z}{2}\right) \quad (6)$$

and at $r_D^{-1}\lambda > 1$ (high salt limit)

$$\psi(z) \approx \pm \frac{2e^{-r_D^{-1}z}}{r_D^{-1}\lambda} \quad (7)$$

In the case of high ionic strength of the solution, the Coulomb contribution to the interaction potential (per monomer unit of the main chain) may be approximated as

$$U_{Coulomb}(z)/k_B T = \alpha\psi(z) \quad (8)$$

where α is the fraction of charged monomers along the backbone. This expression is approximate since it solely describes the electric field (generated by the charged surface) that a probe charge experiences at a certain distance from the surface. However, it does not account for the perturbation caused by the presence of the polyelectrolyte of the electrostatic field created by the charged plane. (Of course, in the numerical SCF calculations, these effects are accounted for.)

As follows from eqs 5–7, and also from Figure 5, the onset of the electrostatic attraction is controlled by the Debye length and therefore depends strongly on the ionic strength of the solution. In Figure 5b, a comparison between the numerical SCF predictions and the analytical curves (eq 5) is presented. The curves for the electrostatic potential from SCF are similar to those from the analytical calculations. Equation 5 provides a good approximation to the exact solution of the PB problem at high ionic strength, but systematically overestimates the strength of electrostatic attraction of the line of charges to the oppositely charged plane for low ionic strength cases.

IV.3. Steric Interaction. Upon the approach of the backbone to the impermeable (repulsive for side chains) surface, spatial restrictions are imposed on the conformations of the grafted chains. As told above, this gives rise to a steric (repulsive) contribution to the effective interaction potential that acts on the molecular brush. More specifically, in the case of a sufficiently small grafting ratio, the confinement of the side chains in this semispace leads to an additional crowding, which enhances the excluded volume interactions between the side chains in the bottle brush.

In order to quantify these effects, we have performed calculations for the bottle brushes with a "phantom" backbone near an uncharged surface and in pure water as a good solvent for the side chains. Calculations were performed for side chains with $n = 45$, 114, and 228 monomer units (corresponding to PEG molecular weights of 2, 5, and 10 kDa, respectively) and three grafting ratios: $g = 2$, 3.5, and 5.

Figure 6 shows the free energy penalty per single side chain (in the y-ordinate, the free energy is multiplied by the grafting ratio) that a neutral *graft*-copolymer encounters when approaching a surface. Two trends can be observed: (i) the free energy penalty increases with the increase in the side chain molecular weight, and (ii) the onset of the repulsive force (i.e., increase in free energy) correlates with the size of the side chains.

There is only a weak grafting ratio dependence observable for the copolymers with the shortest grafts (44 monomer units in our calculations). This means that the side chains interact virtually individually with the surface. The steric repulsive force arises mainly as a result of conformational entropy losses for individual chains confined in a semispace above the surface: this is confirmed by the good superimposition of the curves corresponding to different grafting ratios.

The entropic repulsion arises because of conformational restrictions imposed for single side chains due to the presence of an impermeable surface. (Note that we assume that there is no attractive interaction between the surface and the grafts.) The onset of the steric interaction occurs at a distance from the surface

(40) Pasche, S.; Vörös, J.; Griesser, H. J.; Spencer, N. D.; Textor, M. *J. Phys. Chem. B* **2005**, *109*(37), 17545–17552.

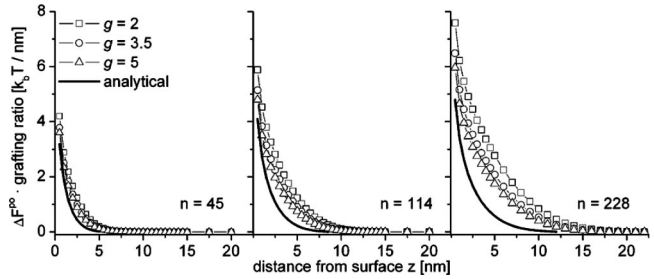

Figure 6. Free energy penalty per grafted side chain of neutral *graft*-copolymers upon approaching a surface for grafts with $n = 45$, 114, and 228. Analytical curves (solid lines) based on eq 9 are also displayed.

that coincides with the size of an unperturbed coil formed by a side chain. Analytically, this contribution can be estimated by

$$U_{\text{conf}}(z)/k_{\text{B}}T = -(1-\alpha)\ \ln[\text{erf}(z/(2R_{\text{g}}))] \qquad (9)$$

when Gaussian chain statistics is assumed. $R_{\text{g}} = (n/6)^{1/2}$ is the radius of gyration of a side chain in the Gaussian coil conformation, and erf(x) is the error function:

$$\text{erf}(x) = 2/\sqrt{\pi}\ \int_0^x \exp(-t^2)\ \text{d}t \qquad (10)$$

The onset of the repulsive potential depends, obviously, on the size of the grafted side chains. The penalty becomes larger the closer the copolymer gets to the surface. As follows from Figure 6, eq 9 systematically underestimates the magnitude of the steric repulsive potential, which points to the contribution of cooperative effects related to enhanced interchain excluded-volume interactions in the bottle brush approaching the impermeable surface. The longer the grafts, the more important are the cooperative effects, as one can clearly see from the departure of the numerically obtained interaction curves from the reference line calculated according to eq 9.

For the copolymers with $n = 114$ and, even more pronounced, with $n = 228$ monomer units per side chains (mimicking PEG(5) and PEG(10) grafts, respectively) the dependence of the grafting ratio is clearly visible. This means that in addition to an entropic penalty imposed to the individual chain, there is a steric (excluded volume) interaction between the side chains (see eq 11), that apparently dominates in the case of densely grafted bottle brushes.

The last contribution to the overall potential is the steric repulsion due to the lateral confinement of the (crowded) side chains in the bottle brush. This interaction is the dominant effect in the case of densely grafted side chains, i.e., at low grafting ratios. When the brush approaches the surface, the *intra*brush steric interactions increase due to the additional crowding of the side chains, leading to a steric free energy penalty. The scaling form of this potential per side chain is

$$\frac{U_{\text{steric}}(z)}{k_{\text{B}}T} = (1-\alpha)\ \frac{(F_{\text{int}} + F_{\text{conf}})}{k_{\text{B}}T}\ \Phi(z/D) \qquad (11)$$

where F_{int} and F_{conf} are the free energies of excluded volume interactions and extension of the grafted chains, respectively. The scaling function $\Phi(x)$ equals zero at $x \geq 1$ (since there is no interaction between the bottle brush and the surface for $z > D$) and increases monotonically for $x < 1$ to reach a finite value on the order of unity at $x = 0$.

IV.4. Total Potential. The shape of the total potential (and thus eventually the adsorption behavior of the polymer) depends on the respective magnitudes of the Coulomb (attractive) and entropic or steric (repulsive) potentials. We present here the interplay of attractive and repulsive (long-range) forces for the case of densely grafted copolymers, where the repulsive part of the potential is dominated by the confinement of the bottle brush (U_{steric}, eq 11).

Table 1. Possible Adsorption Scenarios Depending on the Architectural Parameters of the Copolymer (Grafting Ratio g and Extension of the Side Chains D) and the Environmental Condition (Ionic Strength and Thus Debye Length r_{D})

	conditions	sketch	dominating regime	shape of interaction potential	interpretation
a)	$r_D \geq D$, g ⇑	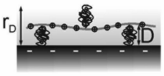	Coulomb $\xi \geq 1$		adsorption
b)	$r_D \geq D$, g ⇓	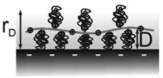	steric $\xi \leq 1$		diffuse, unstable layer
c)	$r_D \leq D$, g ⇑	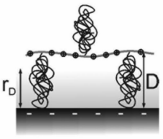	Coulomb $\xi \geq 1$	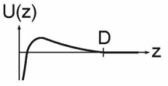	adsorption thermodynamically favorable, but kinetically hindered
d)	$r_D \leq D$, g ⇓	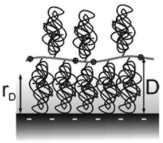	steric $\xi \leq 1$	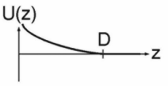	no adsorption

One can imagine different scenarios depending on the copolymer architecture and the environmental conditions. In Table 1 we look into four cases wherein the Debye length $r_{\text{D}} \sim (c_{\text{ions}})^{-1/2}$, the size of the side chains D, and the grafting ratios g are varied. Here, $\xi \cong |U_{\text{Coulomb}}|/U_{\text{steric}}$. Note that this survey is phenomenological in nature and has the purpose to show possible adsorption behaviors.

The four adsorption scenarios presented in Table 1 can be interpreted as follows: (a) For copolymers with a large grafting ratio and with the side chains extensions D smaller than the Debye length r_{D}, a Coulomb-dominated regime arises, which leads to a purely attractive potential $U(z)$ which drives adsorption of the copolymer. (b) For *graft*-copolymers, again with side chain extensions smaller than the Debye length, but with a smaller grafting ratio, the lowering of the linear charge density on the backbone weakens the electrostatic attraction. The steric repulsion, on the other hand, is enhanced as a result of the increased number of side chains as compared to case a. This gives rise to a free energy barrier. Possibly, a strong attraction occurs at very small distances from the surface where electrostatics dominates again. It is very likely that the copolymer remains in the secondary effective potential well and forms a diffuse, unstable interfacial layer. (c) For copolymers with long side chains sparsely grafted to the backbone, the long-range interaction with the surface is dominated by the conformational entropy losses that start at distance D from the surface. At the proximity of the surface, the electrostatic attraction dominates again. The adsorption in such a case is thermodynamically favorable (the absolute minimum of the potential is at the surface), but kinetically hindered because of the free energy barrier that exists due to the conformational entropic penalty for the side chains. (d) For copolymers with long, densely grafted side chains, the steric repulsion dominates

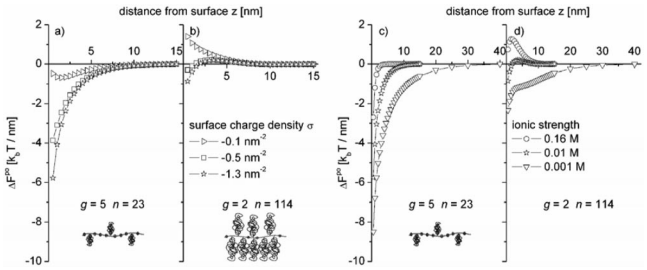

Figure 7. Change in free energy per nanometer of the contour length upon approach of a *graft*-copolymer molecule to the surface. Graphical representations are added that represent the respective polymer architectures. Left: the surface charge density σ is varied between -0.1 and -1.3 nm^{-2} (ionic strength 0.01 M): (a) $g = 5$, $n = 23$, (b) $g = 2$, $n = 114$. Right: the ionic strength is varied between 0.001 and 0.16 M ($\sigma = -1.3$ nm^{-2}): (c) $g = 5$, $n = 23$, (d) $g = 2$, $n = 114$.

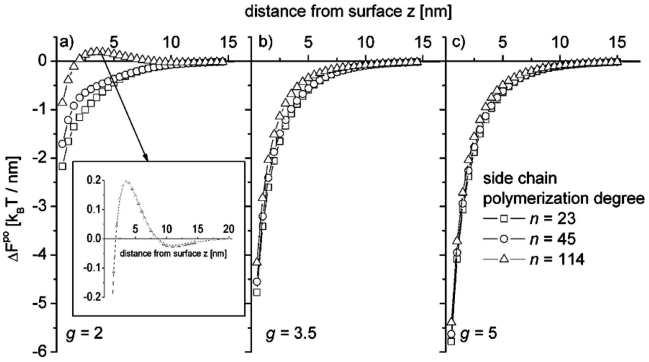

Figure 8. Change in free energy per nanometer of the contour length for different *graft*-copolymer architectures upon approach of a molecule to the surface, showing the effect of different side PEG chain lengths. Ionic strength was 0.01 M, surface charge density -1.3 nm^{-2}. (a) $g = 2$, with an enlarged part of the curve for $g = 2$, $n = 114$ as an inset. Qualitatively, the shape of the curve suggests a thermodynamically favorable, but kinetically hindered adsorption behavior with a certain probability for the molecule to stay in the secondary minimum seen at a distance of about 12 nm from the surface. (b) $g = 3.5$, (c) $g = 5$.

over the Coulomb forces at any distance, and the potential is purely repulsive, leading to no adsorption of the copolymer.

We now analyze how variations in the external conditions affect the total potential. Only two molecular architectures were chosen for this part: $g = 5, n = 23$ and $g = 2, n = 114$ (mimicking PLL-*g*[5]-PEG(1) and PLL-*g*[2]-PEG(5) copolymers, respectively), representing two "extreme" cases: the first one corresponds to a sparse grafting and relatively short side chains, the second one corresponds to a high grafting density and long side chains.

Surface Charge. An ionic strength of 0.01 M and good solvent conditions were applied for the calculations. The parameter varied here was the surface charge density σ. Different scenarios can be seen in Figure 7, where the variation of the free energy as a function of the distance to the surface is plotted for (a) $g = 5$, $n = 23$ and (b) $g = 2$, $n = 114$.

In Figure 7a, all the curves show pure attraction, except for the lowest surface charge density (-0.1 nm^{-2}), where a small repulsion is observed at small distances of the chains to the surface. Nevertheless, all the end-values (when the backbone lies on the surface) still imply adsorption. In the case of the smallest surface charge density ($\sigma = -0.1$ nm^{-2}), the minimum in free energy is at a finite distance away from the surface, which may lead to a diffuse and relatively unstable adsorbed layer. As seen for the electrostatic contribution to the net potential (Figure 5), the end-values change strongly for surface charge densities of magnitude less than $|-0.5|$ nm^{-2}. Note that the shapes of the free energy curves in Figure 7a are similar to the interaction potential schematically presented in Table 1a,b.

In Figure 7b, where the polymer has long, densely grafted side chains, all the curves have a repulsive component. For the lowest surface charge density, the end-value now suggests no adsorption at all, while the other curves end up in the adsorption-favorable range. The magnitude of the values, though, is much smaller than for the other polymer in panel a. Also here, an analogy to the interaction potentials of Table 1c,d is discernible.

Ionic Strength. Next, let us consider for a fixed surface charge density (in units of elementary charges) $\sigma = -1.3$ nm^{-2}, the effect of the ionic strength of the solution. We varied this from 0.001 to 0.16 M. Figure 7c,d again shows the corresponding results for the two polymers: $g = 5, n = 23$ and $g = 2, n = 114$, respectively. Note that the scale for the distance is larger here as compared to Figure 7a,b.

In the case of $g = 5, n = 23$, the onset of the interaction with the surface correlates with the ionic strength of the solution. Clearly, the electrostatic attraction is the dominant contribution to the polymer−surface interaction. The shape of the curves for $g = 2, n = 114$ copolymers are fundamentally different. For all ionic strengths of >0.001 M, there is a repulsive component that increases with increasing ionic strength. The onset of this repulsion is governed by the extension of the side chains and thus arises at the characteristic distance corresponding to the size of the side chains (∼8−10 nm). For the higher salt concentration (0.16 M), the end-value of the curve clearly indicates no adsorption. The 0.001 M curve has very interesting features, showing both electrostatic and steric effects. The onset of the interaction is, similar to the $g = 5$, $n = 23$ case, dictated by the electrostatic attraction at large distances from the surface (∼30 nm). Although the free energy is monotonically decreasing, the shape of the curve is different from the one in Figure 7c. At a distance where the onset of steric repulsion is clearly seen for lower ionic strength, one can identify a leveling off of the attraction before the electrostatic attraction dominates again very close to the surface.

Experimentally Relevant Cases. Here we present results for the adsorption of the bottle brush macromolecules with different architectures aimed to be relevant for experimental cases of the PLL-*g*-PEG molecules with PEG molecular weights of 1, 2, and 5 kDa and grafting ratios of $g = 2$, 3.5, and 5. We choose an ionic strength of 0.01 M, good solvent conditions for the grafts, and a surface charge density of -1.3 nm^{-2}. Figure 8 presents the corresponding change in free energy per nanometer upon bringing the molecule closer to the surface.

For all the cases presented here except of one, the interaction curves show attraction of the polymers to the surface. Only molecules with $g = 2$, $n = 114$ in Figure 8a exhibit a small energy barrier that needs to be overcome in order to adsorb onto the surface. The relevant part of this particular curve is replotted as an inset in Figure 8a. From this inset one can nicely see the secondary minimum at a distance of about 12 nm from the surface, followed by an energy barrier that peaks at around 3 nm from the surface. This type of adsorption behavior corresponds to the thermodynamically favorable, but kinetically hindered case, as presented in Table 1c.

It is evident from these curves that there is no significant effect of the side chain molecular weight for grafting ratios of $g = 3.5$ and 5 (Figure 8b,c), and only the end-values correlate with the grafting ratio. This indicates that the attractive electrostatic effect, which depends on the grafting ratio but not on the molecular weight of the side chains, dominates over the repulsive entropic effect, which depends on the molecular weight of the grafts. Only for densely grafted side chains (grafting ratio $g = 2$, plot 8a), one sees differences between the curves, indicating

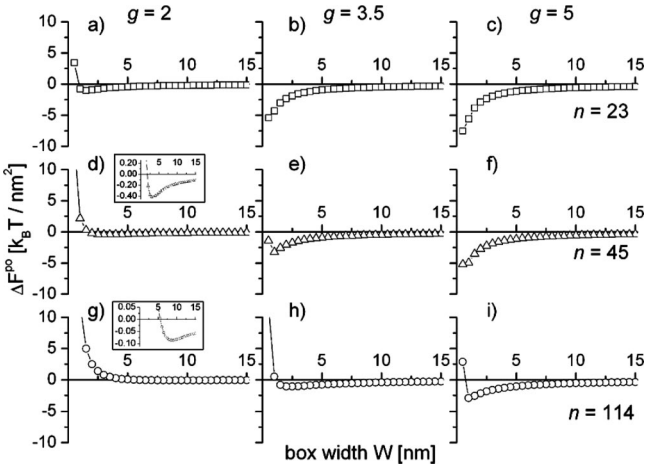

Figure 9. Change in free energy per square nanometer of the surface plotted as a function of the width of the calculation box W (implying the lateral crowding of the adsorbed molecules). W corresponds to half the distance between two polyelectrolyte backbones. As a reference state for the free energy, the value for an unconfined *graft*-copolymer molecule far away from the surface is used. The minimum in these curves corresponds to (thermodynamically) optimal coverage of the surface. Calculations are done for a surface charge density of -1.3 nm^{-2} and ionic strength of 0.01 M. (a,b,c) Polymers with $n = 23$; (d,e,f) $n = 45$ copolymers; (g,h,i) $n = 114$ copolymers. (a,d,g) Results for a grafting ratio of $g = 2$; (b,e,h) for $g = 3.5$; and (c,f,i) for $g = 5$. Panels d and g contain insets that are enlarged graphs that focus on the local minimum in the interaction curves.

the onset of a steric, repulsive bottle brush effect that is able to compete with the electrostatic attraction.

V. Adsorbed Layer Structure on a Surface

V.1. Lateral Crowding of Molecules. The calculations to evaluate the optimal surface coverage, with an account of the lateral crowding of bottle brush molecules adsorbed on the surface, were performed for a surface charge density of -1.3 nm^{-2}, for an ionic strength of 0.01 M and for good solvent conditions for the side chains. We selected molecules with numbers of monomer units $n = 23$, 45, and 114 and grafting ratios $g = 2$, 3.5, and 5. The curves shown in Figure 9 were calculated according to eq 2.

Referring to Figure 9, all the free energy values are normalized with respect to a single molecule in solution far away from the surface, where the molecule neither interacts with its neighbors nor interacts with the surface. Upon decreasing the box width, still at a large distance between neighboring chains, the free energy per unit area monotonically decreases because of a progressive compensation of the surface charge by oppositely charged polyelectrolyte backbone of the molecular brushes. An increase in the free energy found at small values of the box with W arises due to (i) the undercompensation of the steric repulsion of individual chains from the surface by the gain in the electrostatic free energy and (ii) the lateral crowding and hence repulsive interaction between side chains of neighboring molecules. The minimum in the curve approximately corresponds to the thermodynamic equilibrium surface coverage at sufficiently high bulk copolymer concentration, when the translational entropy of the chains in the solution can be safely neglected (plateau regime of the adsorption isotherm).

Curves of Figure 9a,h have a detectable minimum, while curves of Figure 9d,g need an enlargement of the free energy scale to see the minima. The curves of Figure 9b,c,f do not exhibit the increase in free energy at very dense crowding (small W). This does not mean a minimum does not exist in these cases, but

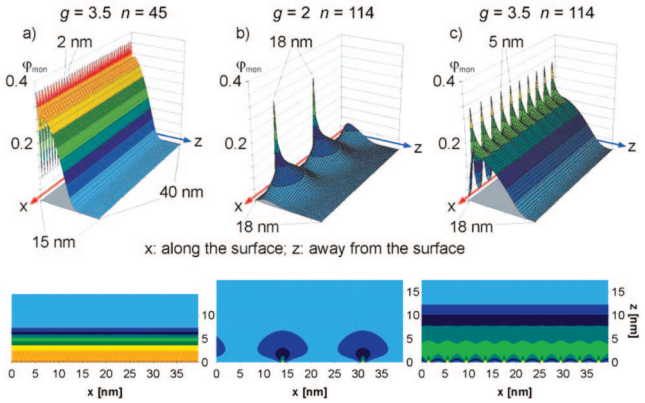

Figure 10. Spatial side chain monomer distributions of adsorbed *graft*-copolymer molecules: (a) $g = 3.5$, $n = 45$, (b) $g = 2$, $n = 114$, (c) $g = 3.5$, $n = 114$. Note that the z-axis has been extended to 18 nm for the copolymers with $n = 114$. Surface charge density is -1.3 nm^{-2}, ionic strength 0.01 M. Top: 3-D plots with the x-axis being the direction along the surface, the z-axis pointing into the solution. φ_{mon} is the volume fraction of side chain monomers. Bottom: 2-D equal-volume fraction contour plots (top view), same data as for the 3-D plots.

rather that we are not able to detect one with the lattice size chosen for these calculations (0.5 nm). This "resolution" problem also appears in curves of Figures 9e,i, where just one repulsive data point value is found. Indeed, the "smoothness" of the well is very poor. This issue will further be discussed when we compare these results with experimental ones later in this section.

V.2. Monomer Distribution Profiles. Since we have access to two-dimensional (2-D) monomer distribution data from the SF-SCF results, we can look into the spatial monomer distributions near the surface upon crowding of the molecules. The three-dimensional (3-D) plots (Figure 10 top) are constructed in the following way: the x-axis shows the distance along the surface in the direction perpendicular to the PLL main chains. The z-axis is the direction perpendicular to the surface plane and points into the solution. The vertical axis in these 3-D plots is always the volume fraction of the side chain monomer units, φ_{mon}. The 2-D plots bottom-graphs (Figure 10) show the same data as the 3-D plots, but now in an equal volume fraction contour plot (mimicking a top-view). These 2-D contour plots give additional insight into the distributions close to the surface, i.e., those parts that are hidden by the peaks of the 3-D plots. The three architectures shown in Figure 10 exhibit rather different monomer distribution patterns. The $g = 3.5$, $n = 45$ copolymers (Figure 10a) adsorb at a small equilibrium interchain distance of only 2 nm, resulting in a very homogeneous layer topography and also high volume fraction values close to the surface ($\varphi_{mon} \approx 0.3$). In contrast, the adsorbed layer of $g = 2$, $n = 114$ molecular brushes (Figure 10b) exhibit a large interchain distance of 18 nm. Apparently, this leads to a rather inhomogeneous lateral monomer distribution, and part of the surface is hardly covered. It should also be noted that, in this particular case, an energy barrier must be overcome by the molecule in order to adsorb onto the surface (see Figure 8). Note that, for Figure 10b,c, the z-axis has been extended to 18 nm because of the higher PEG molecular weight and thus further extension of the side chains. For a larger grafting ratio, i.e., for molecular brushes with $g = 3.5$, $n = 114$ (Figure 10c), the situation is similar to that for $g = 2$, $n = 114$ (Figure 10a), where the surface is densely covered by side chain monomers. Note also the considerably larger chain extension compared to the copolymers with shorter grafts.

It is of considerable interest to focus also on the distributions of the end-segments of the side chains. These volume fraction distributions are shown in Figure 11 for the same polymer

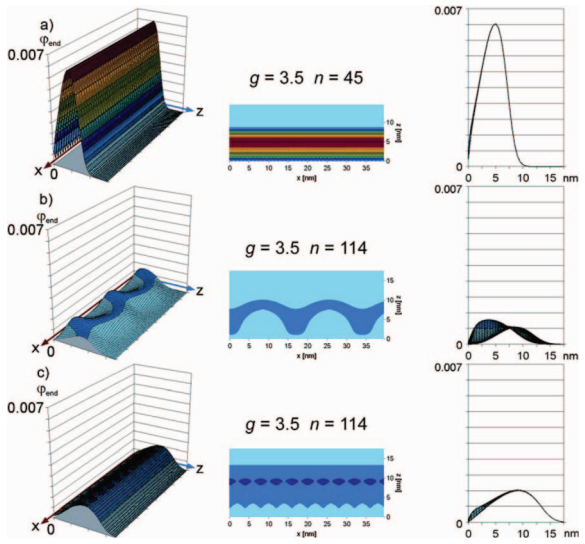

Figure 11. Spatial end-segment monomer distribution of adsorbed *graft*-copolymer molecules. Results are shown for the same architectures and external conditions as in Figure 10. Left: 3-D plots; middle: 2-D contour plots (top view); right: 2-D plot of the volume fraction profile of the end-points $\varphi_{end}(z)$ in the z-direction for all x-values superimposed (side view).

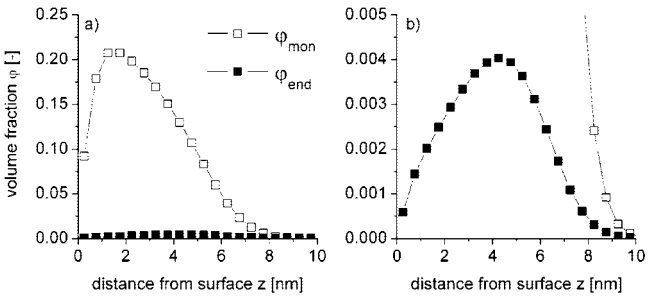

Figure 12. Comparison of volume fraction distributions of side chain monomers and end-segments for $g = 2, n = 45$, i.e., the volume fractions are plotted as a function of the distance from the surface z: (a) the scale on the y-axis is chosen to show the shape of the distribution of the chain segments; (b) the scale on the y-axis has been enlarged in order to show the shape of the distribution of the end-segments and the difference in volume fractions of chain monomers and end-segments at large distances from the surface.

architectures as discussed in Figure 10. The end-segment distribution for the adsorbed layer of $g = 3.5$, $n = 45$ brushes (Figure 11a) is very uniform in the lateral (x-) direction. This is mainly due to the smaller interchain distances as compared to the $g = 2$, $n = 45$ case. For the layer formed by $g = 2$, $n = 114$ brushes (Figure 11b), the distribution is rather wavy, and the absolute values for the volume fractions of the end-segments remain rather low compared to the other cases. The layer of $g = 3.5$, $n = 114$ brushes (Figure 11c), again shows a reasonable homogeneous distribution in the lateral direction. On the right-hand side of Figure 11, we give the distribution of the end-segments as a function of the z-coordinate integrated over the x-coordinate. Clearly in Figure 11b, the spread in end-point distributions is the largest.

In order to get an appropriate picture of the respective volume fractions of the segments of the side chains and their end-segments, both have been plotted on the same ordinate in Figure 12 for the optimum coverage by $g = 2$, $n = 45$ brushes. The values are the average of the lateral volume fraction distributions at a certain value of z. In Figure 12a, one sees that, at any distance from the surface, the volume fraction of the monomers of the side chains is larger than that of the end-segments. In Figure 12b, the ordinate has been rescaled in order to show the shape of the end-segment distribution curve. One also notes that, at the outermost region of the polymer layer (i.e., at $8 < z < 10$ nm), there are more side chain monomers present than end-segments. In fact, the percentage of end-segments (compared with all the present monomers) is highest in this outermost region of the brush, but does not exceed 20%. This is an important result with regard to end-functionalization of *graft*-copolymers for, e.g., biosensing applications. However, we stress that this corresponds to the average distribution under thermodynamic equilibrium, and that dynamic aspects are not treated here.

VI. Discussion and Comparison to Experimental Results

The results of our calculations enable us to rationalize the main qualitative trends observed in experiments for PLL-*g*-PEG adsorption on metal oxide surfaces. Pasche et al.[2] investigated experimentally the systematic relationship that exists between protein repellence of a surface and the EG surface density after PLL-*g*-PEG adsorption, irrespective of PLL and PEG molecular weight. Figure 13 summarizes the PLL(20)-*g*-PEG adsorption measurements performed by optical waveguide lightmode spectroscopy (OWLS), an *in situ* technique sensitive to the dry mass of adsorbates.[41] The polymer concentration in solution was 1 mg/ml, and the ionic strength was 0.01 M. All surfaces were subsequently tested for protein resistance by exposure to serum. The polymer-covered surfaces that resist protein adsorption (<1 ng/cm^2 adsorbed protein mass) are marked with an asterisk (*) in Figure 13.

The number of lysine monomer units adsorbed onto a Nb_2O_5 surface, the number of PEG chains in the adsorbed layer, and the total polymer mass adsorbed are presented in Figure 13a,b,c, respectively, as a function of the inverse grafting ratio, $1/g$ (all the properties are calculated per unit area of the surface). Figure 14 a,b presents the corresponding results of the SCF calculations. Although a quantitative comparison between the experimental results and our SF-SCF calculations is difficult due to the discretization scheme implemented in the SF-SCF calculations, general trends observed in experiments are clearly reproduced and can be rationalized on the basis of our calculations.

As follows from Figures 13a and 14a, for the PEG(1) copolymers, the number of lysine monomer units adsorbed per unit area exhibits a quasi-plateau behavior in a wide range of variation of grafting ratio and is expected to decrease only for very high values of $1/g$. On the contrary, for PEG(2) and PEG(5) copolymers, the number of adsorbed lysine units monotonically decreases as a function of $1/g$. This result implies a strong interplay of electrostatic attractive and steric repulsive forces acting between the PLL-*g*-PEG copolymers and the oppositely charged (adsorbing) surface: a decrease in the fraction of charged monomer units in the PLL chain would imply a larger amount of lysine units per unit area necessary to shield the electrical charge of the surface. In the PEG(1) copolymers this trend is counterbalanced by an increasing steric repulsion due to an increasing fraction of PEG grafts. Furthermore, for PEG(2) and PEG(5) copolymers, the steric repulsion increases strongly upon a decrease in grafting ratio, which leads to a systematic decrease in the amount of adsorbed lysine, except for the range of relatively large grafting ratios.

The discussed above trends in the $1/g$ dependences for the number of lysine monomers adsorbed per unit area manifests in

(41) Vörös, J.; Ramsden, J. J.; Csúcs, G.; Szendro, I.; De Paul, S. M.; Textor, M.; Spencer, N. D. *Biomaterials* **2002**, *23*(17), 3699–3710.

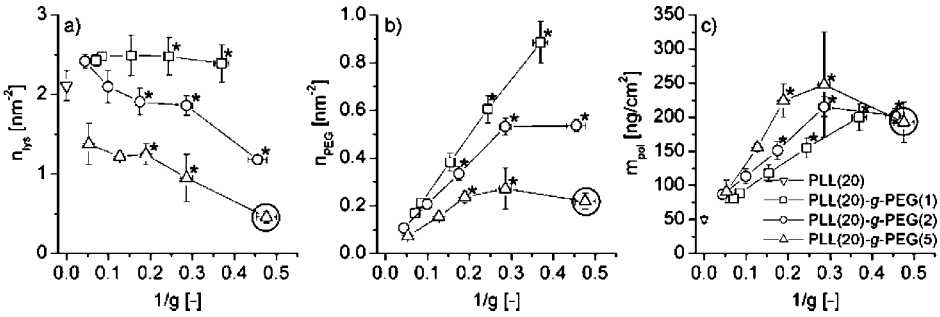

Figure 13. Results from Pasche et al.[2] for PLL-*g*-PEG copolymers with a molecular weight of the PLL main chain of 20 kDa and different grafting ratios and degrees of polymerization of the PEG grafts. (a) The number of lysine monomer units per square nanometer of different PLL-*g*-PEG architectures adsorbed onto Nb_2O_5 (determined by OWLS) plotted as a function of the inverse grafting ratio 1/*g*. (b) The number of PEG chains per square nanometer as a function of the inverse grafting ratio. (c) The adsorbed polymer mass as a function of the inverse grafting ratio. The asterisks (*) denote those surface coverages that resist protein adsorption. The encircled point denotes PLL(20)-*g*[2.1]-PEG(5), which is not protein resistant, even though the amount of adsorbed mass on the surface would suggest protein adsorption resistance.

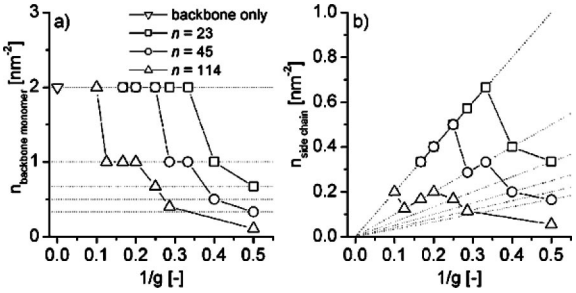

Figure 14. Corresponding data to Figure 13 based on SF-SCF results. (a) The number of polyelectrolyte monomer units per square nanometer of different *graft*-copolymer architectures plotted as a function of the inverse grafting ratio 1/*g*. (b) The number of side chains per square nanometer as a function of the inverse grafting ratio. The dotted lines denote the SF-SCF accessible values for $n_{backbone\_monomer} \geq 0.33$.

the number of PEG chains per unit area in the adsorbed layer: the latter increases quasi-linearly as a function of 1/*g* in the range corresponding to a quasi-plateau behavior for the adsorbed amount of lysine, and levels off or even decreases at large values of 1/*g*. In the latter case, a strong decrease in the number of lysine monomer units per unit area overcompensates an increase in the fraction of lysine units carrying PEG grafts. Remarkably in the range of quasi-linear dependence of the number of PEG chains per unit area on 1/*g*, the larger molecular weight of the PEG grafts correspond to a smaller number of PEG chains per unit area, which again reflects an increasing magnitude of steric repulsion in the adsorbed layer.

Even an analysis of the interaction of a single PLL-*g*-PEG molecule with the surface reveals strong effects that can be traced to the architecture of the copolymers. In the PLL-*g*-PEG copolymer, the number of charges on the PLL backbone (attractive driving force for adsorption onto the surface) is inversely proportional to the number of side PEG chains (the PEG chains cause repulsion from the surface). The onset of crowding of the PEG chains in a PLL-*g*-PEG copolymer (i.e., the transition to the bottle brush regime) seems to depict one case for possibly ideal adsorption conditions. Indeed, the polymer PLL-*g*[2]-PEG(5) is the only one exhibiting a repulsive region in its interaction curve (cf. Figure 8).

From the 2-D analysis of the PEG monomer distribution near the surface, we find a uniform surface coverage for the copolymers with short PEG chains. Reversely, for long PEG chains (e.g., for PLL-*g*[2]-PEG(5), Figure 10b), steric repulsion from the surface and significant interactions between neighboring molecules lead to such low coverages that practically no interpenetration of the PEG coronas occurs. This correlates with the single molecule interaction with the surface, which exhibits a pronounced repulsive component.

The results presented in this work give a new and more detailed insight into the local and large-scale structure of adsorbed PLL-*g*-PEG layers as a function of the relevant architectural parameters. The calculations indicate a change in the behavior for densely grafted copolymers with long side chains with respect to the surface interaction potential and the surface coverage, which is in line with experimental observations of the "special case" of PLL-*g*[2]-PEG(5).

Regarding the protein-repellent behavior of the PLL-*g*-PEG layers, experiments indicate that a complete and uniform coverage of the surface by the copolymer is a requirement. From the point of view of molecular architecture, a too dense grafting of long side chains to the backbone has a clear negative effect on the adsorption behavior of the molecules, eventually leading to a diffuse, unstable layer and probably submonolayer coverage.

Acknowledgment. This project was financed by ETH Zürich (project TH-33./01-3). The support by the French−Swiss Programme d'Actions Intégrées "Germaine de Stael" (Grant No. 13432WK) is acknowledged.

Appendix. SF-SCF Numerical Modeling: Computational Method Description

In order to get a system that is in thermodynamic equilibrium, one needs to establish a (self-consistent) connection between, e.g., the concentration profile of monomers $c(z)$ (z being a spatial coordinate), and the external (mean) field $u(z)$ that acts on the monomers. The general strategy in SCF modeling is to assume a concentration profile $c(z)$ for the monomers, and then associate an average potential $u(z)$ to it that depends on the local concentration $c(z)$.

Subsequently, each chain is described as being subjected to the potential $u(z)$, and all chain properties, such as the statistical weight of the full set of conformations, are computed, resulting in a new value for the concentration profile, $c'(z)$. This procedure is repeated in an iterative way, i.e., a new $u'(z)$ is defined, and chain properties are calculated again until the system converges to a stable solution $c_{final}(z)$. It can then be stated that the potential $u_{final}(z)$ is self-consistent.

The SF-SCF model is based on the Flory−Huggins (FH) mean-field lattice model.[42] The polymer segments are placed on the

(42) Fleer, G. J.; Cohen Stuart, M. A.; Scheutjens, J. M. H. M.; Cosgrove, T.; Vincent, B., *Polymers at Interfaces*; Chapman & Hall: London, 1993.

lattice sites by using a first-order Markov approximation. In the FH theory, a mean field is applied over the whole homogeneous system, which allows the analytical calculation of the partition function for a collection of chains in solution. This, in turn, gives easy access to thermodynamic properties of the system. The fraction of sites occupied by a monomer is denoted as φ and is related to the concentration c (number of monomers per unit volume) by $\varphi = ca^3$, where a^3 is the volume of the unit cell in the cubic lattice.

In the mean-field approximation, the free energy per lattice site can be written as

$$\frac{F_{\mathrm{mix,site}}}{k_{\mathrm{B}}T} = \frac{\varphi}{n}\ln\varphi + (1-\varphi)\ln(1-\varphi) + \chi\varphi\,(1-\varphi) \tag{A1}$$

Here, the free energy of mixing F_{mix} per lattice site is used since it omits certain trivial terms such as terms independent or linear in φ. The first term describes (minus) the translational entropy of the chain (n is the number of monomers in the polymer chain), the second term refers to the translational entropy of the solvent molecules, and the third term refers to the interactions between adjacent molecules (χ is the Flory interaction parameter).

Scheutjens and Fleer[43–45] extended the FH approach by allowing inhomogeneities in one dimension, while the mean-field approximation was maintained in the two remaining directions. This has enabled one to model, e.g., polymers adsorbed or end-grafted onto surfaces of different geometries. Later, this approach was extended by Leermakers et al.[46–48] to two-gradient systems, where segment density fluctuations are accounted for in two directions, while the mean-field approach is applied in the remaining direction. In the following, we will discuss the *basics* of the SF-SCF approach and assume that, e.g., the distributions only depend on the z-coordinate. The extension to more than one gradient is straightforward. Also we will give the most important line of arguments and trust that the many small details, necessary for the numerical implementation of the equations, can be found elsewhere.

The SF-SCF model assumes that the chains are flexible and composed of spherically symmetric segments with characteristic length a. The segments fit on a lattice with corresponding characteristic dimension a. The target of the SCF calculations is to deduce the optimal volume fraction profiles that minimize the free energy of the system under the constraint that the system is incompressible, i.e. $\varphi_{\mathrm{s}}(z) + \varphi(z) = 1$. φ_{s} is the (dimensionless) volume fraction of a monomeric solvent, φ is the volume fraction of the monomer units, and z is a coordinate referring to a set of $L(z)$ lattice sites within which a mean-field averaging is applied.

First, all possible chain conformations on the lattice are methodically generated by a modified Markov-type, step-weighted random-walk procedure, where the a priori step probabilities λ (i.e., the likelihood that a step is taken in a particular direction in the lattice system) are weighted. This means that λ may have different values depending on the direction of the step taken. It is noted here that λ only depends on the lattice geometry, and not on the interaction between chain segments.

Next we introduce the segment weighting factor $G(z)$, where z is the coordinate in the direction where gradients are allowed. $G(z)$ is the statistical weight of having a monomer of the chain in coordinate z or, in other words, stands for the preference of a particular segment for being in layer z. These factors are expressed as Boltzmann factors of the segment potential (ignoring for simplicity the segment type) present in layer z:

$$G(z) = \exp\left(-\frac{u(z)}{k_{\mathrm{B}}T}\right) \tag{A2}$$

where $u(z)$ is the potential of the mean force felt by a segment at distance z. The potential is defined with respect to the bulk solution where all potentials equal zero.

The random-walk procedure is carried out using a so-called recurrence relation that generates the end-segment weighting factors $G(z;s)$, giving the statistical weight of having a chain of length s with its last segment in layer z. The recurrence relation "elongates" a chain of $s-1$ segments into a chain of s segments:

$$G(z;s) = G(z)\{\lambda_{-1}G(z-1;s-1) + \lambda_0 G(z;s-1) + \lambda_1 G(z+1;s-1)\} \tag{A3}$$

where λ_{-1}, λ_1, and $\lambda_0 = 1-\lambda_{-1}-\lambda_1$ are the a priori probabilities to cross to an adjacent layer or to remain in the same layer, respectively. For a polymer of polymerization degree n, s can be seen as a segment ranking number with $s \in [1,n]$ and thus eq A3 can be seen as an end-point distribution function. The part in accolades, often abbreviated as $\langle G(z;s-1)\rangle$, is a step-weighted nearest-neighbor average of the statistical weight of having a chain of length $s-1$ with its last segment $s-1$ at distance z. For our case, we need to introduce two end-point distribution functions in order to account for the asymmetry of our system, i.e., for the fact that one end of our side chain is grafted to the backbone of the main chain:

$$G(z;s|z_1;1) = G(z)\langle G(z;s-1|z_1;1)\rangle \tag{A4}$$

$$G(z;s|n) = G(z)\langle G(z;s+1|n)\rangle \tag{A5}$$

Equation A4 describes the distribution obtained when starting the recurrence relation with segment $s=1$ at coordinate z_1. Note that z_1 indicates that the first segment is fixed (grafted). Equation A5 stands for the distribution obtained when starting from the other end of the chain, i.e. at segment $s=n$. In this case, the location of segment $s=n$ is not specified (is integrated over) since it is the free end of the chain.

From these weighting factors one can calculate the distribution of segment s, $\varphi(z,s)$, using the composition law:

$$\varphi(z,s) = \frac{C}{G(z)}G(z;s|z_1;1)\,G(z;s|n) \tag{A6}$$

where C is a normalization constant. The composition law sums over all possible paths of a polymer of length n passing through position z by the monomer unit with the ranking number s. The monomer weighting factor $G(z)$ in the denominator accounts for the double-counting of segment s. The overall segment distribution

(43) Scheutjens, J.; Fleer, G. J. *J. Phys. Chem.* **1979**, *83*(12), 1619–1635.
(44) Scheutjens, J.; Fleer, G. J. *J. Phys. Chem.* **1980**, *84*(2), 178–190.
(45) Scheutjens, J.; Fleer, G. J. *Macromolecules* **1985**, *18*(10), 1882–1900.
(46) Leermakers, F. A. M.; Scheutjens, J.; Lyklema, J. *Biophys. Chem.* **1983**, *18*(4), 353–360.
(47) Leermakers, F. A. M.; Scheutjens, J. *J. Phys. Chem.* **1989**, *93*(21), 7417–7426.
(48) Leermakers, F. A. M.; Scheutjens, J.; Lyklema, J. *Biochim. Biophys. Acta* **1990**, *1024*(1), 139–151.

$\varphi(z)$ is obtained by summing $\varphi(z,s)$ over all segments of the chain:

$$\varphi(z) = \sum_{s=1}^{n} \varphi(z,s) \tag{A7}$$

The surface is positioned at $z = 0$, and the surface component S has a fixed density: $\varphi_S(0) = 1$ and $\varphi_S(z) = 0$ for $z > 0$. For monomeric components in the system, such as the solvent and the 1:1 electrolyte, the equivalent of eq A6 is simply a Boltzmann equation, where the normalization is given by the volume fraction of this component in the bulk. Note that, in the bulk the incompressibility conditions also apply.

The segment potentials $u(z)$ follow from the overall segment distributions. Physically the segment potential is the work needed to bring the segment from the reference state (bulk) where the potential is zero to the coordinate z. Below we will account for three contributions:

$$u(z) = u'(z) + u^{FH}(z) + u^{el}(z) \tag{A8}$$

The first term is the work needed to create an empty lattice site at z (and giving up one in the bulk). Its value is linked to the incompressibility constraint mentioned above, and therefore the term is also known as the Lagrange field contribution. The second term amounts from the short-range interactions that are parametrized by the Flory χ-parameters. The segment potential depends on the segment type. Hence, for a segment of type A we have

$$u_A^{FH}(z) = k_B T \sum_B \chi_{AB}(\langle\varphi_B(z)\rangle - \varphi_B^b) \tag{A9}$$

where the summation over all segment types in principle includes the surface S, but below we will, for simplicity, ignore all short-range interactions with the surface. The angular brackets account for the nonlocal character of the nearest-neighbor interactions, similarly as in eqs A4 and A5. Again, the normalization with the bulk volume fraction of B is needed to allow the segment potential to be zero in the bulk.

We follow the classical Gouy−Chapman theory to account for the electrostatic contribution to the segment potential. Again, this term depends on the segment type A. Let the valence of segment A be given by α_A, then we can write

$$u_A^{el}(z) = \alpha_A e \Psi(z) \tag{A10}$$

where e is the elementary charge, and $\Psi(z)$ is the local electrostatic potential. The electrostatic potential follows from the Poisson equation. Here and below we will assume that the dielectric constant ε in the solution is homogeneous and fixed. The charge distribution $q(z)$ follows from the volume fraction distributions:

$$q(z) = \sum_A \alpha_A e \varphi_A(z) \tag{A11}$$

Hence, for the flat geometry, the potentials are computed from

$$\frac{\partial^2 \Psi(z)}{\partial z^2} = -\frac{4\pi q(z)}{\varepsilon} \tag{A12}$$

which is straightforwardly implemented on the lattice.

The set of eqs A2 to A12 is closed and routinely solved numerically for a self-consistent solution, up to high precision (at least 7 significant digits). In such a self-consistent solution, the free energy F of the system is computed by

$$F = \sum_z L(z) f(z) \tag{A13}$$

where $L(z)$ refers to the number of lattice sites in layer z, and $f(z)$ is the free energy density, given in its most simple form when there is just a grafted homopolymer in a monomeric solvent:

$$f(z) = \frac{\varphi^b}{n} \ln\left(\frac{N}{G(n|z_1;1)}\right) + \ln(1 - \varphi(z)) + \varphi(z)\chi\langle\varphi(z)\rangle \tag{A14}$$

where φ^b refers to the volume fraction in the bulk, and $G(n|z_1;1)$ is the chain partition function where all conformations are counted that start with segment $s = 1$ in $z = 1$. Obviously, eq A14 is extended by other contributions such as the free energy density due to electrostatic contributions, i.e., $q(z)\Psi(z)/2$, and entropic contributions due to the small ions.

The thermodynamic parameter of interest is the Helmholtz free energy F with the set of ("known" and fixed) independent variables temperature (T), volume (V) and number of particles i in the system (N_i), and the dependent, fluctuating variables entropy (S), pressure (p) and chemical potential of the species i, (μ_i).

In our SCF calculations, however, we focus on the so-called partial open free energy F^{po}, defined as

$$F^{po} = F - \sum \mu_{mobile} N_{mobile} \tag{A15}$$

where the summation is performed over all the mobile components in the system (i.e., solvent molecules, ions, but not the polymer chains). The system (or volume for which the calculations are performed) is connected to a reservoir with a fixed volume fraction of ions and solvent molecules (and thus also fixed chemical potentials). Contrary to the chain monomers, the solvent molecules and ions are free to exchange between the system and the reservoir, which is the reason why the free energy is called "partial open". This ensures, e.g., electroneutrality of the system when one introduces charges on the polymer chain. At the last layer in the system we have implanted reflecting boundary conditions.

LA800272V